Dark Matter Phenomenology from the Holographic Bit-Mode Balance Framework

Dávid Nagy *

Posted Date: 23 March 2026

doi: 10.20944/preprints202603.1770.v1

Keywords: Holographic Bit-Mode Balance; HBMB; dark matter; holographic principle; local screens; Bekenstein-Hawking entropy; filament profiles; weak lensing; cosmic filaments; Wheeler-DeWitt equation; self-energy correction; radial acceleration relation; MOND; emergent gravity; spectral truncation; soft cutoff; pseudo-isothermal density profile

 doi:10.20944/preprints202603.1770.v1

Article

Dark Matter Phenomenology from the Holographic Bit–Mode Balance Framework

Dávid Nagy

Independent Researcher, Hungary; dave.nagy.86@gmail.com

Abstract

The gravitational excess phenomena commonly attributed to dark matter are usually explained in standard cosmology by introducing a non-baryonic matter component. In this work we examine a different route within the Holographic Bit–Mode Balance (HBMB) framework. The core HBMB principle is that Bekenstein–Hawking entropy is not merely an informational upper bound, but an actual bound on physical resolution and on the number of independent bulk modes that can be assigned to a local screen or horizon. As a result, bulk reconstruction is naturally capacity-limited and spectrally truncated, while the large-ℓ sector does not disappear through a sharp cutoff; instead, it remains present as an accessibility-weighted soft remainder. The present version sharpens the central HBMB claim by identifying the primary analytic object as a three-dimensional effective density profile,

$$\rho_{\mathrm{HBMB}}(r) = \frac{\rho_0}{r^2 + r_0^2},$$

rather than by postulating the projected filament profile directly. For cylindrical filament geometry this yields the observable projected profile

$$\Sigma_{\mathrm{fil}}(R) = \frac{\pi\rho_0}{\sqrt{R^2 + r_0^2}},$$

which has a finite core and an R^{-1} wing, consistent with the standard cylindrical $\beta = 2/3$ benchmark used in part of the filament-stacking literature. In parallel, we formulate an alternative local-screen route based on WDW self-energy corrections and an α-fixpoint-like capacity–demand selection principle. In that route, tidal and density/Poisson screen selectors yield physically reasonable local screen scales, while a Schur-complement-motivated second-order closure,

$$g_{\mathrm{HBMB}} = \xi\,\frac{a_*^2}{g_{\mathrm{bar}}}, \qquad a_*(x) = \frac{c^2}{\sqrt{N_c}\,R_*(x)},$$

produces a toy-model low-acceleration slope consistent with the RAR/MOND-like 1/2 scaling, although a full SPARC-level validation is deferred to future work. The paper therefore presents two complementary HBMB testing routes: a filament-profile route that is immediately observable in stacking and lensing, and a local-screen galaxy route that provides a concrete mechanistic path toward galaxy-scale phenomenology.

Keywords: Holographic Bit-Mode Balance; HBMB; dark matter; holographic principle; local screens; Bekenstein-Hawking entropy; filament profiles; weak lensing; cosmic filaments; Wheeler-DeWitt equation; self-energy correction; radial acceleration relation; MOND; emergent gravity; spectral truncation; soft cutoff; pseudo-isothermal density profile

 doi:10.20944/preprints202603.1770.v1

1. Introduction

1.1. The Dark Matter Problem as a Phenomenological Question

One of the most fundamental open problems in modern astrophysics and cosmology is to understand the origin of gravitational effects that do not follow from visible baryonic matter alone. Galaxy rotation curves, gravitational lensing maps, cluster dynamics, and large-scale cosmic structure all contain observations that point to an effective excess of gravity. The standard interpretation explains this by postulating a new, predominantly non-baryonic matter component: dark matter.

Although this picture has been phenomenologically successful in many contexts, the ultimate physical nature of dark matter remains open. It is therefore legitimate to ask whether at least part of the observed gravitational excess might arise not from a new particle sector, but from the structure of the gravitational description itself, or from the informational and reconstructive structure associated with spacetime. This paper investigates that possibility within the Holographic Bit–Mode Balance framework, in a broader conceptual landscape that includes thermodynamic and holographic approaches to gravity such as Jacobson's horizon-thermodynamic argument and later emergent-gravity programs [4,12]. Within the HBMB program itself, the present dark-matter paper is also meant to connect back to the earlier local-screen and scale-setting results obtained in the α-fixpoint and holographic-vacuum-energy works [17,18].

1.2. The HBMB Viewpoint: Horizon-Bit Capacity and Bulk Reconstruction

The basic HBMB idea is that the bit capacity associated with a local screen or horizon is not merely an abstract informational quantity, but a real limit on physically representable bulk structure [15,16]. In this view, the Bekenstein–Hawking entropy [1,2]

$$S(R) = \frac{A(R)}{4\ell_P^2} \tag{1}$$

assigned to a boundary surface of characteristic radius R is not only an upper bound, but also limits the maximal number of independent bulk modes. In HBMB, the bulk is therefore not a primary continuum of arbitrarily fine resolution; instead, it is an emergent description shaped by screen capacity, mode structure, and reconstruction accessibility.

This has a decisive consequence for the present paper. If bulk reconstruction is capacity-limited, then the observable mass density and gravitational response need not coincide with classical matter distribution in the naive sense. Part of the observed excess may instead be the imprint of how a physical system can be represented and reconstructed from a local holographic boundary.

1.3. Neither Particle DM Nor MOND as an Axiom

The present approach deliberately departs from two common starting points. First, we do not introduce a new dark-matter particle as an axiom. Second, we do not assume a MOND-like interpolation law or a predefined acceleration relation [3]. Our goal is not to rewrite a known alternative scheme, but to ask whether the spectral reconstruction structure of HBMB can by itself generate a dark-matter-like effective gravitational excess.

This is methodologically important. If MOND-like or other emergent-gravity relations appear at galaxy or filament scales, we treat them as consequences rather than postulates. The main question of this paper is therefore not how HBMB can be made to fit an already chosen alternative gravity formula, but what effective observable profile follows from horizon capacity, mode budget, and the accessibility-weighted high-ℓ sector.

1.4. Why Can HBMB Produce a Dark-Matter-Like Effect?

If the capacity associated with a local screen limits the representable bulk mode structure, then the high-resolution sector must necessarily be modified. The large-ℓ sector need not vanish completely; rather, it becomes progressively inaccessible or weighted. As a result, projected observables – such

 doi:10.20944/preprints202603.1770.v1

as surface mass density or lensing convergence – can differ from what an unbounded, infinitely resolved bulk description would suggest. The WDW-based HBMB regularization further shows that the omitted high-ℓ sector can induce a self-energy-like correction on the retained sector, with a residual effect controlled by screen capacity [19]. This provides strong motivation to interpret dark-matter-like phenomena as the structured difference between the accessible and omitted sectors.

1.5. Main Claim and Focus of the Present Work

The central claim of this paper is no longer formulated directly at the level of the projected filament profile. Instead, we take the primary HBMB object to be an effective three-dimensional density profile,

$$\rho_{\mathrm{HBMB}}(r) = \frac{\rho_0}{r^2 + r_0^2}, \tag{2}$$

where r is a three-dimensional distance variable, ρ_0 is a normalization constant, and r_0 is a characteristic HBMB core scale. The directly observable filament profile then follows from cylindrical projection,

$$\Sigma_{\mathrm{fil}}(R) = \int_{-\infty}^{+\infty} \rho_{\mathrm{HBMB}}\left(\sqrt{R^2 + z^2}\right) dz = \frac{\pi \rho_0}{\sqrt{R^2 + r_0^2}}, \tag{3}$$

so that the measurable filament wing decays as R^{-1} rather than R^{-2}. This makes the HBMB filament prediction compatible, at the level of asymptotic shape, with the widely used cylindrical $\beta = 2/3$ benchmark [5,7].

At the same time, the paper develops a second and more local route: a WDW-inspired self-energy picture in which a local screen is selected by a capacity–demand balance in the spirit of the HBMB α-fixpoint logic, and the omitted-sector correction is converted into an effective extra acceleration through a Schur-complement-motivated response closure. In the present draft this local-screen route is still exploratory, but it already yields physically plausible screen scales and a toy-model low-acceleration $1/2$ slope.

The primary focus of the paper remains the filament scale and the associated lensing observables. Galaxy rotation curves and possible MOND-like relations are treated as a secondary but now more explicit consistency program, while a full treatment of cluster mergers lies outside the immediate scope of the present version.

1.6. Structure of the Paper

Section 2 summarizes the minimal HBMB ingredients needed for discussing dark-matter-like phenomena. Section 3 introduces the effective dark matter mechanism in HBMB language. Section 4 shows how a minimal HBMB soft-tail picture can be organized at the level of a three-dimensional core density and cylindrical filament projection, and relates that derivation to the representative-kernel language of the recent WDW results. Throughout the paper, every newly introduced symbol is explained locally at first use so that the derivation remains easy to follow. Sections 5 and 6 provide the validation framework for filaments and lensing observables. Section 7 gives both a spherical toy extension and an alternative local-screen route motivated by WDW self-energy corrections, Section 8 positions the cluster-scale problem, and Section 9 compares the proposal with ΛCDM, MOND-like phenomenology, and other emergent-gravity approaches.

2. Minimal HBMB Ingredients for Describing Dark-Matter-Like Phenomena

2.1. The Horizon as a Physical Capacity Surface

The starting point of HBMB is that a boundary surface, screen, or local horizon associated with a physical system is not merely a geometric auxiliary notion, but an object that determines the actual capacity of the physical description. In this picture, Bekenstein–Hawking entropy is not only an informational upper bound, but an effective limit on the number of physically accessible and

 doi:10.20944/preprints202603.1770.v1

representable degrees of freedom [15,16]. In other words, the area of the horizon not only permits, but constrains how many independent modes can appear stably and reconstructibly in the bulk.

2.2. Capacity and Mode Counting: the HBMB Reconstruction Logic

A central HBMB ingredient is the direct link between horizon capacity and the number of bulk modes. In a spherical or locally angular decomposition, the number of reconstructable modes up to maximal angular order is approximately

$$N_{\mathrm{mode}}(\ell_{\max}) = (\ell_{\max} + 1)^2. \tag{4}$$

This quantity is constrained by screen or horizon capacity, which naturally leads to an effective spectral cutoff,

$$\ell_{\max}(R) \approx \sqrt{S(R)} - 1, \tag{5}$$

possibly up to $O(1)$ geometric or normalization factors [15]. The WDW formalism sharpens this logic into

$$(L(R) + 1)^2 = N_{\mathrm{acc}}(R) + \nu, \tag{6}$$

where N_{acc} is the redundancy-free accessible mode count and $\nu > 0$ is a soft residual seed regularizing the near-saturated limit [19]. This refinement is useful for the dark matter direction as well, because it explicitly distinguishes the formally available mode budget from the physically accessible one.

2.3. Soft Cutoff Instead of a Hard Cutoff

The above relation might seem to suggest a sharp spectral truncation: modes with $\ell \leq \ell_{\max}$ survive, while modes with $\ell > \ell_{\max}$ are simply absent. But that would be too rigid and does not match either the operational HBMB viewpoint or the earlier HBMB intuition about the physical role of high-ℓ sectors.

In HBMB, accessibility of modes associated with local screens and horizons is generally not binary. High-resolution modes are not necessarily forbidden; rather, they become gradually less representable, less stable, or less relevant as redundancy-free physical carriers. The natural HBMB implementation is therefore not a hard cutoff but a *soft cutoff*: an effective weighting that progressively suppresses the large-ℓ sector.

2.4. Local Screens and Operational Horizons

Within HBMB, a screen or local horizon is an operational notion rather than a metaphor. It is a boundary surface to which one can simultaneously assign:

1. capacity or entropy,
2. mode counting,
3. physical accessibility,
4. and a bulk reconstruction rule.

These local screens are not isolated independent objects; rather, they can be understood as nested and overlapping code surfaces of a larger reconstruction structure. In that nested-horizon picture, smaller screens are not separate universes or separate entropy budgets, but local partial encodings within a broader code geometry.

2.5. Redundancy-free Modes and Accessibility Weights

A subtle but crucial HBMB point is that not every formally allowed mode carries the same physical content. The relevant question is not only how many modes can be written down mathematically, but how many of them encode *redundancy-free, physically accessible* information. This distinction leads naturally to accessibility weights. In the high-ℓ sector, formal degeneracy alone does not imply equal physical contribution; capacity and boundary accessibility imply that the effective weight of large-ℓ

 doi:10.20944/preprints202603.1770.v1

modes must decrease. Yet the decrease is not a jump to zero – it is gradual. That graduality is one of the keys to the HBMB dark matter mechanism.

2.6. What the WDW Perspective Contributes

The recent WDW-based HBMB regularization contributes two important lessons. First, the raw geometric overlap does not directly determine the correct physical kernel; rather, one must isolate the redundancy-free accessible channel. Second, the elegant exactly summable kernel should not be read as a unique microscopic truth, but as a representative member of a broader asymptotic universality class [19]. The dark matter paper adopts exactly that logic: the exponential tail is not claimed to be the only possible HBMB kernel, but the simplest precisely tractable representative of a physically motivated soft-tail class.

2.7. Transition to an Effective Tail Description

From the HBMB standpoint, the key question for dark-matter-like phenomena is not simply whether there exists an effective cutoff, but how the high-ℓ sector remains present in observable quantities. In the remainder of this paper we operationalize this via an effective accessibility-weighted tail function. The goal is not to replace the full microscopic reconstruction, but to encode the minimal HBMB structure in a form directly tied to projected observables.

3. The Effective Dark Matter Mechanism in HBMB

3.1. What Do We Mean by "Dark Matter" in HBMB Language?

In the standard interpretation, dark matter is an additional gravitating component beyond baryonic matter. In the HBMB framework we ask the question differently. Rather than assuming that the excess must come from a new particle sector, we start from the fact that the observable bulk response is already the result of a capacity-limited reconstruction tied to local screens. In this sense, "dark matter" is not primarily a type of matter, but the phenomenological name for the observed gravitational excess.

In the present work, the HBMB effective dark matter mechanism means that the bit capacity associated with a local screen or horizon, the corresponding spectral truncation, and the redundancy-free accessibility-weighted high-ℓ sector together generate a projected mass-density and lensing profile that, in standard analysis, appears as extra gravitating matter. The emphasis is on the word *effective*: the observed excess need not come from a separate microscopic particle population, but may follow from the fact that bulk description is itself screen-limited rather than infinitely resolved.

3.2. The Difference between Classical and HBMB Bulk Descriptions

In a classical viewpoint, a mass distribution, potential, or density field can in principle be described at arbitrarily fine resolution. If the fitted gravitational response is larger than what baryonic matter alone would produce, the simplest interpretation is to add another mass component. In HBMB, however, the starting representation is already modified.

Suppose a physical system is associated with a local screen or horizon of characteristic radius R_H. Then the corresponding capacity,

$$S(R_H) = \frac{A(R_H)}{4\ell_P^2}, \tag{7}$$

constrains the maximal number of independent bulk modes. Here $A(R_H)$ is the screen area, ℓ_P is the Planck length, and R_H is not necessarily a cosmological horizon; in the present paper it denotes a general effective local screen scale. The reconstructed bulk description is therefore not identical to a hypothetical classical bulk with unlimited spectrum. The difference becomes especially important in the high-resolution sector, where progressively fewer of the formally available modes carry redundancy-free, operationally accessible physical content.

 doi:10.20944/preprints202603.1770.v1

3.3. Truncated Reconstruction as a Source of Effective Excess

In HBMB, truncation is not simply information loss or a technical limitation; it is part of the physical mode of representation. If a given screen has finite capacity, then reconstruction of bulk fields must take place in some truncated or weighted spectral basis. The dark-matter-like excess therefore appears not as an extra component added at the end, but as the structured difference between the reconstructed profile and the classical fully resolved one.

In WDW language, one may phrase this by saying that the omitted high-ℓ sector induces a Schur-complement-type self-energy correction on the retained accessible sector [19]. In the present dark matter context we do not use that structure at the full minisuperspace-operator level, but at the level of projected profiles: the observable excess is interpreted as the effective, capacity-controlled difference between the retained and omitted sectors.

3.4. Redundancy-free Accessibility and Effective Spectral Weights

Let us denote the effective accessibility weight of spectral modes by p_ℓ in the angular language or $W(k)$ in the continuum transverse language. Here ℓ is angular order and k is the transverse wavenumber conjugate to the filament cross-section. These quantities encode the relative contribution of high-resolution modes once local screen capacity and edge-sector accessibility are taken into account.

The relevant physical point is this: the formal degeneracy of large-ℓ modes may be high, but the redundancy-free, actually accessible fraction does not increase without bound. Capacity and local screen accessibility imply that the effective weight of the large-ℓ sector decreases, but not abruptly to zero. Here ℓ denotes angular multipole order, p_ℓ the corresponding discrete accessibility weight, and $W(k)$ the continuum accessibility weight for transverse wavenumber k. That gradual decrease is the key to the HBMB dark matter mechanism.

3.5. GR Compatibility: Left-Hand Side or Right-Hand Side?

Phenomenologically, the present paper treats the HBMB contribution as an effective source term. That is, we parametrize the observed excess through

$$G_{\mu\nu} = 8\pi G\left(T^{\rm bar}_{\mu\nu} + T^{\rm HBMB,eff}_{\mu\nu}\right). \tag{8}$$

Here $G_{\mu\nu}$ is the Einstein tensor, $T^{\rm bar}_{\mu\nu}$ is the baryonic source term, and $T^{\rm HBMB,eff}_{\mu\nu}$ is the *effective* contribution arising from screen-limited reconstruction. Ontologically this is not particle dark matter, but reconstruction-induced excess; phenomenologically it may behave like an effective dark-matter halo. In short: *phenomenologically equivalent to an effective DM halo, but ontologically distinct from particle dark matter*.

3.6. Why Does This Appear as Mass Density?

A natural question is why we may talk about effective mass density at all if the mechanism is non-particle-based. The answer is that gravitational lensing and many astrophysical measurements do not directly measure particles; rather, they measure the imprint of curvature and projected gravitational response. If a model yields the same observable $\Sigma(R)$, $\kappa(R)$, $\gamma_t(R)$, or $g_{\rm eff}(r)$, then at the phenomenological level it explains the same "excess" regardless of whether it derives that excess from new matter or from an emergent reconstruction effect.

3.7. The Central Role of Projection

One of the central claims of this paper is that the HBMB dark-matter-like effect becomes visible most cleanly in projected observables. In filament geometry, the relevant signal is concentrated in the transverse cross-section. The spectral tail is therefore mapped directly into the shape of $\Sigma(R)$, where R is the transverse distance from the filament axis and $\Sigma(R)$ is the projected surface mass density. This makes cosmic filaments the most natural first testing ground for the HBMB dark matter mechanism.

 doi:10.20944/preprints202603.1770.v1

3.8. The Minimal HBMB Mechanism in One Line

The minimal HBMB dark matter mechanism used in this paper can be summarized schematically as

$$\text{screen capacity} \longrightarrow \text{spectral cutoff} \longrightarrow \text{accessibility-weighted tail} \longrightarrow \Sigma(R),\ \kappa(R),\ \gamma_t(R). \quad (9)$$

Here $\kappa(R)$ is the lensing convergence and $\gamma_t(R)$ the tangential shear. In WDW-inspired notation one may additionally associate an amplitude modulation,

$$\Delta U_{\mathrm{HBMB}}(R) \propto \frac{1}{N_{\mathrm{acc}}(R)+\nu}, \qquad \Delta U^{\mathrm{ren}}_{\mathrm{HBMB}}(R) \propto \frac{1}{(N_{\mathrm{acc}}(R)+\nu)(1+N_{\mathrm{acc}}(R)/N_c)}, \quad (10)$$

where $N_{\mathrm{acc}}(R)$ is the redundancy-free accessible mode count, $\nu > 0$ is the soft residual seed, and N_c is a critical scale for capacity-suppressed mixing [19]. In the present manuscript we do not yet use this directly as a fitting formula, but we take it as an important HBMB pattern: both the amplitude and the shape of the effective excess depend on accessible capacity.

3.9. What Is Not Claimed at This Stage?

For methodological clarity it is equally important to state what we are *not* claiming here. We do not claim that HBMB in its present form already solves the full dark matter problem on all scales. Nor do we claim that the filament profile automatically implies all galaxy rotation curves or a complete description of cluster mergers. The purpose of the present section is much narrower: to formulate clearly how an effective projected gravitational excess can arise from HBMB already at the minimal structural level.

4. HBMB Soft Cutoff, the Three-Dimensional Core Profile, and Filament Projection

4.1. Notation and Strategy

We now reorganize the HBMB derivation in a way that is both geometrically cleaner and more directly comparable to the filament literature. The primary HBMB object is taken to be an effective three-dimensional density profile $\rho_{\mathrm{HBMB}}(r)$. The observable filament profile $\Sigma_{\mathrm{fil}}(R)$ is obtained only after cylindrical projection along the line of sight. Here r denotes the three-dimensional distance from the filament axis, R the observed transverse distance in the sky plane, and z the line-of-sight coordinate so that $r^2 = R^2 + z^2$.

The role of the WDW paper in the present section is structural rather than literal. It tells us that the omitted high-ℓ sector induces a genuine self-energy correction on the accessible sector, that the physical correction is controlled by redundancy-free accessibility, and that elegant exactly summable kernels should be interpreted as representatives of a broader asymptotic class rather than as unique microscopic truths [19]. We therefore use the nested-screen semigroup only as a minimal HBMB axiomatization for the shape of the soft tail, while the direct observable profile is obtained after projection of the resulting three-dimensional effective density.

4.2. What WDW Says – and What It Does Not

In the WDW regularization, the renormalized omitted-sector determinant takes the large-L form

$$\Gamma^{\mathrm{ren}}_{Q}(L) = \Gamma_0 - \frac{2}{3}\ln L - \frac{31}{360}L^{-2} + O(L^{-4}), \quad (11)$$

where L is the accessible multipole threshold, $\Gamma^{\mathrm{ren}}_{Q}(L)$ is the renormalized omitted-sector determinant, Γ_0 is an L-independent constant, and the logarithmic and L^{-2} terms describe the residual running after subtraction of bulk-like and code-boundary contributions [19]. Under a minimal unit-response closure this leads to an effective amplitude

$$\rho_{\mathrm{HBMB}}(L) = \rho_\infty \exp\Big[-c_\chi\, g^{-1}_{\mathrm{eff}}(L)\Big], \qquad g^{-1}_{\mathrm{eff}}(L) = g_R^{-1} + \frac{2}{3}\ln\frac{L}{L_0} + \frac{31}{360}L^{-2} + O(L^{-4}). \quad (12)$$

 doi:10.20944/preprints202603.1770.v1

It follows directly that

$$\rho_{\mathrm{HBMB}}(L) \sim L^{-\frac{2}{3}c_\chi} \qquad (L \to \infty). \tag{13}$$

This is the first important lesson: the logarithmic WDW running does not by itself imply an exponential momentum-space tail. What WDW supports instead is the existence of a soft omitted-sector correction, a rank-one accessible channel, and a representative-kernel or universality-class viewpoint.

4.3. Nested-screen Composition as a Minimal HBMB Axiomatization

Let $\mathcal{A}(k;s)$ denote the effective accessibility weight that the transverse mode k survives in the redundancy-free sector after a coarse-graining depth or screen-composition parameter s. We do not claim that the relation

$$\mathcal{A}(k;s_1+s_2) = \mathcal{A}(k;s_1)\,\mathcal{A}(k;s_2) \tag{14}$$

is a unique microscopic theorem of HBMB. Rather, we adopt it as the minimal scale-consistent and Markov-like implementation of the idea that successive nested-screen coarse-graining steps further suppress redundancy-free transverse accessibility. Under continuity in s, the Cauchy functional equation gives

$$\mathcal{A}(k;s) = e^{-s\psi(k)}, \tag{15}$$

with a nonnegative generator $\psi(k)$.

In the filament cross-section, isotropy and parity imply that the generator can only depend on $|k|$, namely $\psi(k) = \psi(|k|)$. This leads to the stable class

$$W_\beta(k) = W_0 \exp\Big[-(r_0|k|)^\beta\Big], \qquad 0 < \beta \le 2, \tag{16}$$

where W_0 is an overall amplitude, r_0 a characteristic core scale, and β labels the universality class of the transverse generator. In this language, the semigroup structure is not presented as the only possible HBMB completion, but as the simplest nested-screen accessibility model that is both analytically tractable and directly falsifiable.

4.4. Why the $\beta = 1$ Choice Is Physically Preferred in the Present Paper

The choice

$$\psi(|k|) = |k| \qquad \Longleftrightarrow \qquad W(k) = W_0 e^{-r_0|k|} \tag{17}$$

is not claimed to be the only possible HBMB kernel. It is preferred here for two linked reasons. First, it is the simplest nontrivial isotropic generator compatible with the rank-one collective tangential channel emphasized by the WDW analysis. Second, it is the unique member of the stable class that gives an algebraic, rather than Gaussian, spatial wing. In other words, the $\beta = 1$ choice is not justified by mathematical simplicity alone, but because it provides a concrete, data-distinguishable prediction: finite cores together with slow algebraic wings in projected filament observables.

At the same time, an important technical distinction must be made. A direct unweighted three-dimensional Fourier transform of the minimal exponential generator does *not* by itself yield the pseudo-isothermal density exactly. In the present paper we therefore do not identify

$$W(k) = W_0 e^{-r_0|k|} \tag{18}$$

with a raw three-dimensional Fourier pair of

$$\rho_{\mathrm{HBMB}}(r) = \frac{\rho_0}{r^2 + r_0^2}. \tag{19}$$

Rather, the pseudo-isothermal core density is used as the effective coarse-grained real-space representative of the same HBMB algebraic tail class, after the redundancy-free phase-space weighting

 doi:10.20944/preprints202603.1770.v1

implied by projected screen reconstruction. A full first-principles derivation of that momentum-space weighting is left to a later version of the program.

Assume that nested-screen coarse-graining acts on redundancy-free transverse accessibility through the minimal semigroup axiomatization above, and let the preferred representative be the $\beta = 1$ member of the stable class. Then the corresponding HBMB three-dimensional core profile is taken, at the effective coarse-grained level, to be represented by

$$\rho_{\mathrm{HBMB}}(r) = \frac{\rho_0}{r^2 + r_0^2}, \tag{20}$$

where ρ_0 is an amplitude and r_0 a core scale. Cylindrical projection then yields the directly observable filament profile

$$\Sigma_{\mathrm{fil}}(R) = \frac{\pi \rho_0}{\sqrt{R^2 + r_0^2}}. \tag{21}$$

4.5. Three-Dimensional Core Profile and Filament Projection

The HBMB primary object is the three-dimensional effective density

$$\rho_{\mathrm{HBMB}}(r) = \frac{\rho_0}{r^2 + r_0^2}. \tag{22}$$

Here r is the three-dimensional distance to the filament axis and r_0 is the HBMB core scale. To obtain the filament observable one projects along the line of sight,

$$\Sigma_{\mathrm{fil}}(R) = \int_{-\infty}^{+\infty} \rho_{\mathrm{HBMB}}\left(\sqrt{R^2 + z^2}\right) dz, \tag{23}$$

with $r^2 = R^2 + z^2$. Substituting the HBMB profile gives

$$\Sigma_{\mathrm{fil}}(R) = \int_{-\infty}^{+\infty} \frac{\rho_0}{R^2 + z^2 + r_0^2}\, dz. \tag{24}$$

Using the standard integral

$$\int_{-\infty}^{+\infty} \frac{dz}{z^2 + a^2} = \frac{\pi}{a}, \qquad a > 0, \tag{25}$$

with $a^2 = R^2 + r_0^2$, one obtains

$$\boxed{\Sigma_{\mathrm{fil}}(R) = \frac{\pi \rho_0}{\sqrt{R^2 + r_0^2}}.} \tag{26}$$

The profile therefore has a finite core, $\Sigma_{\mathrm{fil}}(0) = \pi \rho_0 / r_0$, and an asymptotic wing

$$\Sigma_{\mathrm{fil}}(R) \sim R^{-1} \qquad (R \gg r_0). \tag{27}$$

This is precisely the asymptotic behavior of the standard cylindrical $\beta = 2/3$ benchmark used in part of the filament-stacking literature [5,7].

4.6. Spherical Analogue and Asymptotically Flat Rotation Curves

The same three-dimensional HBMB profile can also be used in a sphericalized toy model. The enclosed mass is

$$M_{\mathrm{HBMB}}(r) = 4\pi \int_0^r \frac{\rho_0 r'^2}{r'^2 + r_0^2}\, dr' = 4\pi \rho_0 \left(r - r_0 \arctan \frac{r}{r_0} \right). \tag{28}$$

 doi:10.20944/preprints202603.1770.v1

The corresponding circular speed is

$$v_c^2(r) = \frac{GM_{\mathrm{HBMB}}(r)}{r} = 4\pi G\rho_0\left(1 - \frac{r_0}{r}\arctan\frac{r}{r_0}\right). \tag{29}$$

For $r \gg r_0$ one has $\arctan(r/r_0) \to \pi/2$, so

$$v_c^2(r) \to 4\pi G\rho_0, \tag{30}$$

that is, the profile naturally gives asymptotically flat rotation curves in the spherical toy extension. This does not yet constitute a SPARC-level fit, but it shows that the same three-dimensional HBMB core profile can underlie both the filament projection and the basic flat-curve heuristic.

4.7. Representative Kernel and Asymptotic Class

For physical interpretation of the result, an important methodological lesson from the WDW paper should be emphasized. There the kernel

$$K_\ell(R) = \beta(R)\,\frac{2\ell+1}{\ell^2(\ell+1)^2} \tag{31}$$

is special because it is exactly summable,

$$\sum_{\ell=L+1}^{\infty}\frac{2\ell+1}{\ell^2(\ell+1)^2} = \frac{1}{(L+1)^2}, \tag{32}$$

but the WDW paper interprets it not as a unique microscopic derivation, but as an exactly summable representative of the correct asymptotic class [19]. We use precisely the same logic here. The $\beta = 1$ transverse tail is not necessarily the unique HBMB kernel, but a minimal analytically tractable representative of a broader accessibility-controlled stable class.

4.8. Rank-one Collective Channel and Correction to Naive Geometry

The WDW results also emphasize that the retained coarse mode communicates not with many independent microchannels, but with a uniform tangential collective mode. This means that physical kernel scaling is not determined by the raw geometric strip-overlap, but by redundancy-free channel averaging. In the present dark-matter paper this intuition appears as the statement that the effective tail weight leading to the filament density profile comes not from the full formal high-ℓ degeneracy, but from the accessible collective mode sector. The projected R^{-1} filament wing is therefore not merely a fitting convenience, but a geometrically consistent signature of a three-dimensional HBMB core profile combined with cylindrical projection.

4.9. Alternative Tail Classes and Their Observational Differences

The preferred HBMB profile should be understood as the representative of a wider class. Different stable generators lead to different three-dimensional profiles and therefore to different projected filament shapes. The $\beta = 1$ class yields an algebraic projected wing $\Sigma_{\mathrm{fil}} \sim R^{-1}$ after cylindrical projection. A Gaussian-like generator would instead produce a much steeper wing, while other $0 < \beta < 2$ stable classes would lead to different Lévy-type families. The filament profile therefore carries direct information about the accessibility class of the high-ℓ sector.

 doi:10.20944/preprints202603.1770.v1

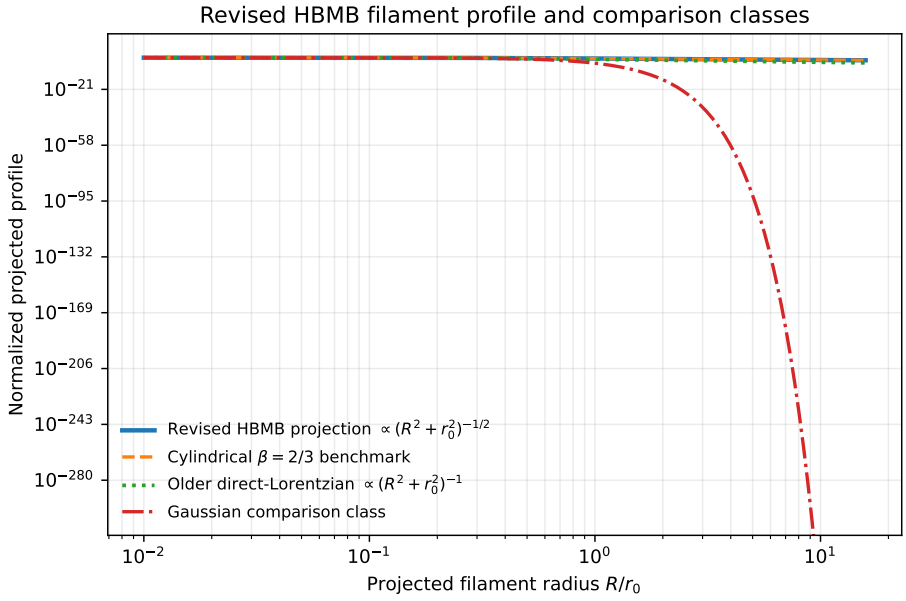

Figure 1. Comparison of the revised HBMB filament prediction with common reference profiles. The primary HBMB object is the three-dimensional core density $\rho_{\mathrm{HBMB}}(r) \propto (r^2 + r_0^2)^{-1}$. Cylindrical projection then yields $\Sigma_{\mathrm{fil}}(R) \propto (R^2 + r_0^2)^{-1/2}$, i.e. an R^{-1} wing, unlike the older direct-Lorentzian projection with R^{-2} wings.

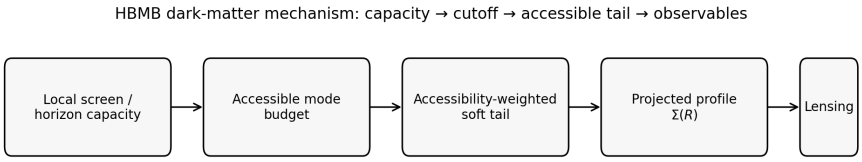

Figure 2. Revised HBMB pipeline. Screen capacity constrains the accessible mode budget; accessibility-weighted high-ℓ remnants generate a three-dimensional HBMB core density, whose cylindrical projection gives the directly observable filament profile.

5. Filament Observations and Validation Strategy

5.1. What Is the Directly Testable Prediction?

With the revised formulation the directly testable filament prediction is

$$\Sigma_{\mathrm{fil}}(R) = \frac{\pi \rho_0}{\sqrt{R^2 + r_0^2}}, \tag{33}$$

where R is the projected transverse separation from the filament axis, ρ_0 is the three-dimensional HBMB density amplitude, and r_0 is the HBMB core radius. This profile has a finite core and an asymptotic R^{-1} wing. It should therefore be compared not to a direct two-dimensional Lorentzian ansatz, but to cylindrical filament benchmarks such as the projected $\beta = 2/3$ profile used in part of the filament-stacking literature [7].

5.2. Why Are Filaments Especially Suitable?

Filaments remain the cleanest first testing ground because their geometry is close to cylindrical, the transverse profile is directly observable through stacking and lensing, and the comparison class is simple. The point of the present paper is not yet to show that HBMB solves all dark-matter phenomenology, but to provide a sharply falsifiable first prediction at filament scale.

 doi:10.20944/preprints202603.1770.v1

5.3. Suggested Validation Pipeline

A concrete validation program should proceed as follows. First, construct stacked transverse profiles from a filament catalogue. Second, fit the revised HBMB projected profile

$$\Sigma_{\rm fil}(R) = \frac{\pi\rho_0}{\sqrt{R^2 + r_0^2}} \tag{34}$$

against the relevant observable or its lensing proxy. Third, compare the inferred r_0 and goodness of fit with standard cylindrical reference profiles, including the $\beta = 2/3$ benchmark and Gaussian-like alternatives. Fourth, test whether the same r_0 range is compatible with the spherical toy analogue used for galaxy-scale intuition.

5.4. What Should the Numerics Demonstrate?

At minimum the numerics should show: (i) that the revised projected HBMB profile can fit realistic filament stacks with sensible core radii; (ii) that the R^{-1} wing is distinguishable from steeper alternatives over the available dynamic range; and (iii) that the inferred filament core scale is not wildly inconsistent with the galaxy-scale illustrative extension. In practice, the most immediate comparison set is the existing filament-stacking literature, including the tSZ and lensing analyses of de Graaff et al. and Xia et al. [6,8].

6. Lensing Observables

6.1. Surface Density and Convergence

For the revised filament profile the directly relevant lensing quantity is the projected surface density itself,

$$\Sigma_{\rm fil}(R) = \frac{\pi\rho_0}{\sqrt{R^2 + r_0^2}}, \tag{35}$$

with corresponding convergence

$$\kappa(R) = \frac{\Sigma_{\rm fil}(R)}{\Sigma_{\rm crit}} = \frac{\pi\rho_0}{\Sigma_{\rm crit}\sqrt{R^2 + r_0^2}}. \tag{36}$$

Here $\Sigma_{\rm crit}$ is the usual critical surface density of lensing geometry [21]. Since the present paper focuses on cylindrical filament observables, we treat Σ and κ as the primary directly testable quantities.

6.2. Shape-only Tests

A useful normalization-free diagnostic is the profile ratio

$$\mathcal{R}(R; R_{\rm ref}) \equiv \frac{\Sigma_{\rm fil}(R)}{\Sigma_{\rm fil}(R_{\rm ref})} = \sqrt{\frac{R_{\rm ref}^2 + r_0^2}{R^2 + r_0^2}}. \tag{37}$$

This isolates the shape and core scale independently of the overall amplitude. The observable distinction between the HBMB profile and steeper alternatives is then encoded in the slow R^{-1} wing and in how rapidly the profile leaves the finite-core regime.

6.3. A Note on Cylindrical Versus Spherical Lensing Quantities

At filament scale the central observable is the cylindrical projected density itself. A more complete cylindrical lensing treatment can be added in a later version if needed, but the present prediction is already directly comparable to stacked filament measurements reported as transverse projected profiles.

 doi:10.20944/preprints202603.1770.v1

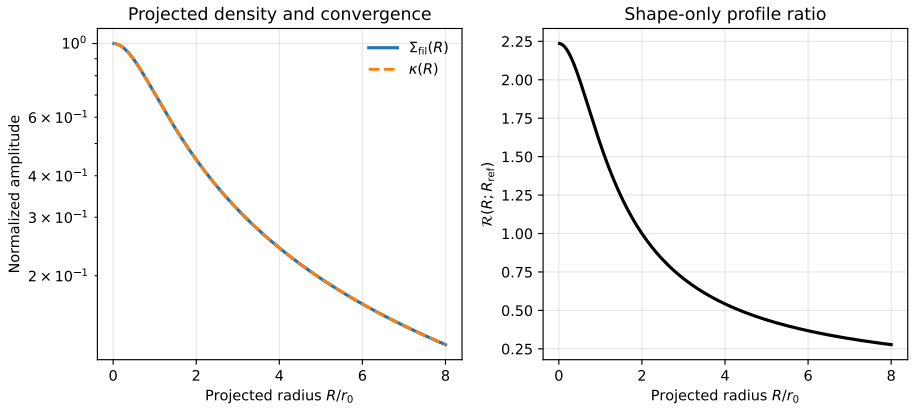

Figure 3. Revised filament observables. Left: the projected HBMB filament profile $\Sigma_{\rm fil}(R) \propto (R^2 + r_0^2)^{-1/2}$. Right: the corresponding convergence shape after division by a fiducial $\Sigma_{\rm crit}$.

7. Illustrative Galaxy-Scale Extension and Explicit Observational Benchmark

7.1. Why Only a Secondary Validation Layer?

The galaxy-scale discussion remains secondary in the present paper. The filament route is currently the sharper and more directly testable prediction. The galaxy section is included because the same three-dimensional HBMB core profile and the WDW/local-screen route suggest a concrete, potentially testable path toward RAR-like behavior, even though no full SPARC-level fit is yet claimed. In that sense the relevant benchmark is not simply the existence of asymptotically flat curves, but the full low-scatter galaxy phenomenology encoded in modern rotation-curve compilations such as SPARC [13].

7.2. A Spherical Analogue of the HBMB Core Profile

The spherical analogue of the filament core density is simply

$$\rho_{\rm HBMB}(r) = \frac{\rho_0}{r^2 + r_0^2}. \tag{38}$$

As shown in Section 4, this yields an enclosed mass

$$M_{\rm HBMB}(r) = 4\pi\rho_0 \left(r - r_0 \arctan \frac{r}{r_0} \right) \tag{39}$$

and an asymptotically flat circular speed. This remains only an illustrative sphericalization, not a replacement for full disk modeling.

7.3. An Alternative Local-Screen Route from WDW Self-Energy

The more interesting galaxy-scale route starts from the WDW observation that the omitted high-ℓ sector induces a self-energy-like correction controlled by the redundancy-free accessible sector [19]. Inspired by the HBMB α-fixpoint logic, we do not select the relevant local screen by hand. Instead we introduce a capacity–demand balance: a local screen radius $R_*(x)$ is selected by requiring a dimensionless gravitational mode-demand factor to become order unity.

The simplest acceleration/Rindler choice,

$$\Xi_a(R;x) = \frac{g_{\rm bar}(x) R}{c^2}, \tag{40}$$

leads to

$$R_*^{(a)}(x) = \frac{c^2}{g_{\rm bar}(x)}, \tag{41}$$

 doi:10.20944/preprints202603.1770.v1

which is generally too large to be useful on galaxy scales. We therefore focus on two more promising selectors:

$$\Xi_t(R;x) = \frac{R^2|\nabla g_{\rm bar}(x)|}{c^2}, \qquad R_*^{(t)}(x) = \frac{c}{\sqrt{|\nabla g_{\rm bar}(x)|}}, \tag{42}$$

and

$$\Xi_\rho(R;x) = \frac{4\pi G\rho_{\rm bar}(x)R^2}{c^2}, \qquad R_*^{(\rho)}(x) = \frac{c}{\sqrt{4\pi G\rho_{\rm bar}(x)}}. \tag{43}$$

Here $g_{\rm bar}(x)$ is the baryonic acceleration, $|\nabla g_{\rm bar}(x)|$ its local gradient, and $\rho_{\rm bar}(x)$ the local baryonic density. In toy galaxy examples both the tidal and density/Poisson selectors produce local screen radii of order a few to ten Mpc, whereas the acceleration/Rindler choice runs to implausibly large scales.

Given such a selected screen, we define a local WDW-inspired response scale

$$a_*(x) = \frac{c^2}{\sqrt{N_c}\, R_*(x)}, \tag{44}$$

where N_c is the critical accessible-capacity scale already appearing in the WDW omitted-sector decoupling factor. This response scale can then be converted into an effective extra acceleration in several possible ways.

7.4. Response Closures and Toy RAR Scaling

Three closures are particularly natural to test. The first is a simple additive scale,

$$g^{(1)}_{\rm HBMB} = a_*. \tag{45}$$

The second is a geometric-mean closure,

$$g^{(2)}_{\rm HBMB} = \sqrt{g_{\rm bar}a_*}. \tag{46}$$

The third, and most interesting, is a Schur-complement-motivated second-order closure,

$$\boxed{g^{(3)}_{\rm HBMB} = \xi\,\frac{a_*^2}{g_{\rm bar}}}, \tag{47}$$

with a dimensionless normalization factor ξ. The motivation is that the WDW effective operator correction is second order in the retained–omitted coupling, so a ratio of the form $a_*^2/g_{\rm bar}$ is structurally more natural than an ad hoc MOND interpolation.

For a point-mass toy galaxy both the tidal and density selectors imply

$$R_*(r) \propto \frac{r^{3/2}}{\sqrt{M}}, \qquad a_*(r) \propto \frac{\sqrt{M}}{r^{3/2}}, \tag{48}$$

so that at fixed mass one has

$$a_*(r) \propto g_{\rm bar}^{3/4}. \tag{49}$$

It follows that

$$g^{(1)}_{\rm HBMB} \propto g_{\rm bar}^{3/4}, \qquad g^{(2)}_{\rm HBMB} \propto g_{\rm bar}^{7/8}, \qquad g^{(3)}_{\rm HBMB} \propto g_{\rm bar}^{1/2}. \tag{50}$$

Thus only the Schur-complement closure yields the deep-RAR/MOND-like low-acceleration slope of $1/2$ in the toy model. This is not yet a full RAR solution – thin-disk geometry, realistic SPARC mass models, and first-principles values of ξ and N_c remain open – but it provides a genuine HBMB mechanism rather than a mere phenomenological interpolation.

 doi:10.20944/preprints202603.1770.v1

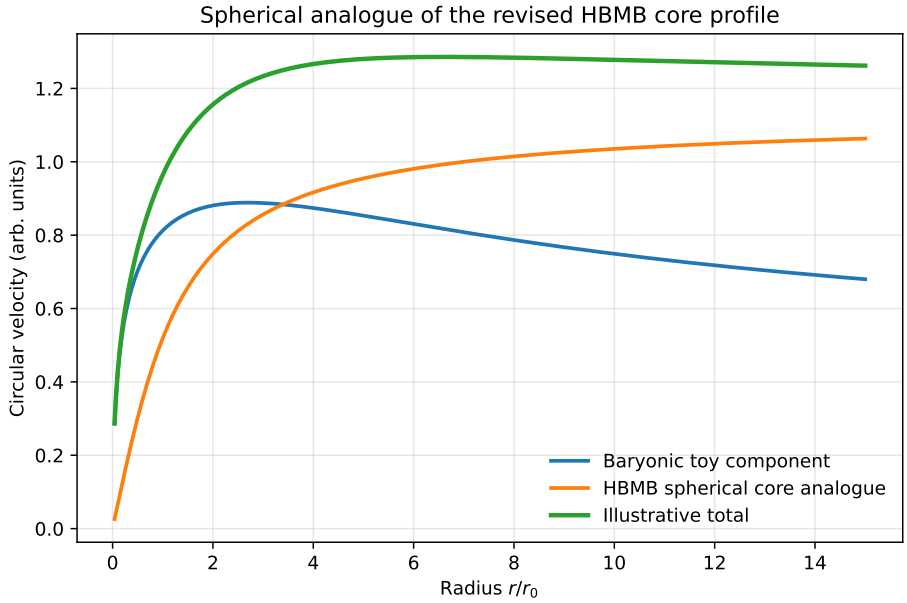

Figure 4. Illustrative galaxy-scale consequences of the revised HBMB picture. The sphericalized HBMB core density yields asymptotically flat curves, while the alternative local-screen route gives a toy-model low-acceleration $1/2$ slope only for the Schur-complement-inspired closure $g_{\mathrm{HBMB}} = \xi a_*^2/g_{\mathrm{bar}}$.

7.5. Relation to RAR and MOND-like Phenomenology

The present draft therefore makes a more precise claim than before. We do not claim that HBMB already solves the full radial acceleration relation, nor that the thin-disk SPARC geometry has been implemented. What we can already say is that an α-fixpoint-like local-screen selection principle, together with the WDW critical-capacity scale and a Schur-complement-type second-order closure, yields a concrete HBMB path toward a low-acceleration $1/2$ slope without inserting a MOND interpolation formula by hand.

8. Cluster Scales and Merging Systems

Cluster mergers remain the most difficult regime for any non-particle interpretation of dark-matter phenomenology. In the present HBMB program we do not claim a solved Bullet-Cluster derivation. However, the local-screen language suggests a more concrete working hypothesis than in the earlier draft. The effective HBMB excess need not track the collisional X-ray gas directly; instead it may track the evolving nested screen network associated with the dominant potential and curvature structure. During a merger the shocked gas is decelerated hydrodynamically, while the collisionless galaxy component and the dominant potential ridges continue more ballistically. If the HBMB effective sector follows the screen-network geometry rather than the gas density itself, then lensing peaks can in principle remain closer to the galaxy/potential centroids than to the gas bullet, in qualitative analogy with the offset highlighted in the Bullet Cluster literature [9,10].

This is still a working hypothesis rather than a complete derivation, and a dedicated merger simulation would be required to test it. The point of including it here is only to make explicit that the HBMB program does have a concrete route to a gas–lensing offset: the screen network may advect and relax differently from the collisional baryonic plasma.

9. Comparison with ΛCDM, MOND-like Phenomenology, and Verlinde's Emergent Gravity

9.1. Difference between ΛCDM and HBMB

In ΛCDM, dark-matter-like phenomena are primarily explained by a non-baryonic halo component, often parameterized at galaxy and halo scales by profiles of NFW type [20]. In HBMB, by contrast, the gravitational excess arises from the combined effect of screen capacity, mode budget, the

 doi:10.20944/preprints202603.1770.v1

accessibility-weighted high-ℓ tail, and projection. The two pictures may meet at the level of observable quantities, but the underlying mechanism is different.

9.2. MOND as an Emergent Benchmark

MOND is famously strong on galaxy scales because it naturally yields flattened rotation curves and scaling relations closely related to the baryonic Tully–Fisher relation [3,14]. The HBMB dark matter direction does not start from MOND, but from its own reconstruction logic. If MOND-like relations appear, they are consequences rather than assumptions. In particular, the RAR provides a direct empirical benchmark that any HBMB galaxy-scale completion must eventually confront.

9.3. Relation to and Difference from Verlinde's Theory

Erik Verlinde's emergent gravity program treats dark-matter-like phenomena in terms of de Sitter background structure, entropy displacement, and an additional gravitational response [12]. Weak-lensing tests of Verlinde-type apparent dark matter have also been discussed in the literature [11]. HBMB and Verlinde share a broad motivational ground, and both can be placed in a lineage that also includes Jacobson's horizon-thermodynamic perspective [4]. The main difference is that HBMB builds the origin of dark-matter-like phenomena explicitly from local screen capacity, mode counting, and an accessibility-weighted spectral tail. Whereas Verlinde's picture is primarily formulated in terms of an excess acceleration and entropy displacement, HBMB works in the language of *spectral accessibility* and *projected observables*.

9.4. Falsifiability

One of the main strengths of the HBMB proposal is that it provides concrete shape tests:

- a projected HBMB filament core together with an algebraic R^{-1} wing,
- stability of the best-fit R_0 across different samples,
- mutual consistency of $\Sigma(R)$, $\kappa(R)$, and $\gamma_t(R)$,
- distinguishability from alternative tail classes,
- and the test whether the representative-kernel-inspired accessible/omitted split organizes the data better than raw geometric scaling.

If these shape tests systematically fail, then at least the present minimal HBMB soft-tail implementation is falsified.

10. Conclusions

In the present paper we have sharpened the HBMB dark-matter program in two important ways. First, the primary HBMB object is now the three-dimensional core density

$$\rho_{\mathrm{HBMB}}(r) = \frac{\rho_0}{r^2 + r_0^2}, \tag{51}$$

rather than the projected filament profile itself. Cylindrical projection then yields the directly observable filament prediction

$$\Sigma_{\mathrm{fil}}(R) = \frac{\pi \rho_0}{\sqrt{R^2 + r_0^2}}, \tag{52}$$

which has a finite core and an R^{-1} wing. This puts the filament section on a geometrically cleaner footing and aligns it with standard cylindrical benchmarks used in the filament-stacking literature.

Second, the galaxy-scale discussion is now more explicit about the alternative local-screen route suggested by the WDW self-energy picture. In that route, tidal and density/Poisson selectors provide physically sensible local screen radii, the WDW critical capacity defines a local response scale,

$$a_*(x) = \frac{c^2}{\sqrt{N_c} R_*(x)}, \tag{53}$$

 doi:10.20944/preprints202603.1770.v1

and a Schur-complement-motivated second-order closure,

$$g_{\rm HBMB} = \xi \, \frac{a_*^2}{g_{\rm bar}}, \tag{54}$$

yields a toy-model low-acceleration $1/2$ slope. We do not claim that this already constitutes a full SPARC/RAR solution, but it does provide a concrete and testable HBMB mechanism rather than a purely phenomenological interpolation.

The recent WDW results continue to strengthen the program in structural terms. They clearly separate the accessible and omitted sectors, show that the large-ℓ remainder induces a self-energy-like correction on the accessible sector, and emphasize that elegant exactly summable kernels should be interpreted as representatives of a universality class rather than as unique microscopic truths [19]. The present paper therefore uses WDW logic as structural support for both the filament route and the local-screen galaxy route, while keeping the directly testable filament prediction at the center of the current draft.

The main goal of the next version is to implement the concrete filament-stacking comparison numerically with the revised projected profile, to derive the required momentum-space weighting that would connect the exponential accessibility generator to the effective pseudo-isothermal core profile from first principles, and to test the local-screen route against realistic galaxy data rather than only against toy models.

Appendix A. Additional Remarks on the Interpretation of the Soft Cutoff

In the present manuscript the semigroup construction is not used as a microscopic proof, but as a minimal nested-screen accessibility model. The physically observable filament profile is not identified directly with the semigroup kernel. Instead, the semigroup logic motivates a three-dimensional HBMB core density, and the directly observable filament profile is obtained only after cylindrical projection. A full first-principles derivation of the required redundancy-free momentum-space measure is reserved for a later version of the program.

Appendix B. Closed Forms for the Revised Filament Projection

Starting from

$$\rho_{\rm HBMB}(r) = \frac{\rho_0}{r^2 + r_0^2}, \qquad r^2 = R^2 + z^2, \tag{A1}$$

one obtains by direct projection

$$\Sigma_{\rm fil}(R) = \int_{-\infty}^{+\infty} \frac{\rho_0 \, dz}{R^2 + z^2 + r_0^2} = \frac{\pi \rho_0}{\sqrt{R^2 + r_0^2}}. \tag{A2}$$

The corresponding convergence is

$$\kappa(R) = \frac{\pi \rho_0}{\Sigma_{\rm crit} \sqrt{R^2 + r_0^2}}, \tag{A3}$$

and the normalization-free profile ratio is

$$\mathcal{R}(R; R_{\rm ref}) = \sqrt{\frac{R_{\rm ref}^2 + r_0^2}{R^2 + r_0^2}}. \tag{A4}$$

Appendix C. A WDW-Inspired Methodological Remark

A useful lesson from WDW regularization is that the raw omitted-tail sum should not be treated as directly observable. It is preferable to separate bulk-like, interface/code-boundary, and true residual

 doi:10.20944/preprints202603.1770.v1

contributions. In later, data-driven versions of the dark matter paper this viewpoint will likely become important for disentangling background/core structure from the genuinely observable tail signal.

Appendix D. Summary of Notation and Variables

The main quantities are the following. r is the three-dimensional distance from the filament axis or spherical center, R is the observed transverse distance in the sky plane, and z is the line-of-sight coordinate, with $r^2 = R^2 + z^2$ for cylindrical projection. The HBMB core density amplitude is ρ_0 and the three-dimensional core scale is r_0. The projected filament profile is $\Sigma_{\rm fil}(R) = \pi\rho_0/\sqrt{R^2 + r_0^2}$. In lensing, $\kappa(R) = \Sigma_{\rm fil}(R)/\Sigma_{\rm crit}$ is the convergence.

In the local-screen route, $R_*(x)$ denotes the selected local screen radius, N_c the WDW critical accessible-capacity scale, and

$$a_*(x) = \frac{c^2}{\sqrt{N_c} R_*(x)} \tag{A5}$$

the corresponding HBMB local response scale. The extra toy-model acceleration is denoted by $g_{\rm HBMB}(x)$, while $g_{\rm bar}(x)$ is the baryonic acceleration.

Appendix E. Reproducibility and Python Scripts

The accompanying code package is available at https://github.com/davenagy86/HBMB_DarkMatter and serves four purposes. First, the scripts generate illustrative figures for the filament projection and its comparison to alternative profile classes. Second, they verify the distinction between WDW-inspired residual running and the semigroup-based accessibility model. Third, they implement the local-screen selection models (acceleration, tidal, and density/Poisson). Fourth, they demonstrate the toy galaxy closures, including the Schur-complement-inspired $g_{\rm HBMB} = \xi a_*^2/g_{\rm bar}$ route that yields a low-acceleration $1/2$ slope in the point-mass toy model. All figures in the present paper can be reproduced from the scripts in this repository.

References

1. J. D. Bekenstein, Black Holes and Entropy, *Physical Review D* **7**, 2333–2346 (1973).
2. S. W. Hawking, Particle Creation by Black Holes, *Communications in Mathematical Physics* **43**, 199–220 (1975).
3. M. Milgrom, A modification of the Newtonian dynamics as a possible alternative to the hidden mass hypothesis, *Astrophysical Journal* **270**, 365–370 (1983).
4. T. Jacobson, Thermodynamics of Spacetime: The Einstein Equation of State, *Physical Review Letters* **75**, 1260–1263 (1995), arXiv:gr-qc/9504004.
5. A. Cavaliere and R. Fusco-Femiano, X-rays from hot plasma in clusters of galaxies, *Astronomy & Astrophysics* **49**, 137–144 (1976).
6. A. de Graaff, Y.-C. Cai, C. Heymans, and J. A. Peacock, Missing baryons in the cosmic web revealed by the Sunyaev–Zel'dovich effect, *Astronomy & Astrophysics* **624**, A48 (2019), arXiv:1709.10378.
7. H. Tanimura, N. Aghanim, F. Bonjean, et al., A search for warm/hot gas filaments between pairs of SDSS LRG galaxies, *Astronomy & Astrophysics* **643**, A136 (2020).
8. Q. Xia, Y. Luo, Q. Guo, et al., A gravitational lensing detection of filamentary structures connecting luminous red galaxies, *Astronomy & Astrophysics* **633**, A89 (2020), arXiv:1909.05852.
9. M. Markevitch, A. H. Gonzalez, D. Clowe, et al., Direct constraints on the dark matter self-interaction cross section from the merging galaxy cluster 1E0657–56, *Astrophysical Journal* **606**, 819–824 (2004), arXiv:astro-ph/0309303.
10. D. Clowe, M. Bradac, A. H. Gonzalez, et al., A direct empirical proof of the existence of dark matter, *Astrophysical Journal Letters* **648**, L109–L113 (2006), arXiv:astro-ph/0608407.
11. M. M. Brouwer, M. A. Troxel, E. A. Macaulay, et al., First test of Verlinde's theory of emergent gravity using weak gravitational lensing measurements, *Monthly Notices of the Royal Astronomical Society* **466**, 2547–2559 (2017), arXiv:1612.03034.
12. E. P. Verlinde, Emergent Gravity and the Dark Universe, *SciPost Physics* **2**, 016 (2017), arXiv:1611.02269.
13. F. Lelli, S. S. McGaugh, and J. M. Schombert, SPARC: Mass Models for 175 Disk Galaxies with Spitzer Photometry and Accurate Rotation Curves, *Astronomical Journal* **152**, 157 (2016).

 doi:10.20944/preprints202603.1770.v1

14. S. S. McGaugh, F. Lelli, and J. M. Schombert, The Radial Acceleration Relation in Rotationally Supported Galaxies, *Physical Review Letters* **117**, 201101 (2016), arXiv:1609.05917.
15. D. Nagy, Basics of a Geometry-Independent HBMB Holographic Principle: From Horizon Bits to Bulk Wavefunctions—Part I, *Preprints* **2026**, 202601.1465 (2026).
16. D. Nagy, U(1)-Driven Local Holographic Horizons: Holographic Bit–Mode Balance and the α-Fixpoint, *Preprints* **2026**, 202511.1803 (2026).
17. D. Nagy, A First-Principles Derivation of the Fine-Structure Constant from Holographic Bit–Mode Balance, OSF Preprints (2025), osf.io/hw2je.
18. D. Nagy, Holographic Vacuum Energy from Quantized Horizons, OSF Preprints (2025), osf.io/m8t6h.
19. D. Nagy, *Holographic Bit–Mode Balance Regularization of Wheeler–DeWitt Cosmology: Determinant Running and Inflationary Closure*, *Preprints* **2026**, 2026031311 (2026). https://doi.org/10.20944/preprints202603.1311.v1.
20. J. F. Navarro, C. S. Frenk, and S. D. M. White, A Universal Density Profile from Hierarchical Clustering, *Astrophysical Journal* **490**, 493–508 (1997).
21. P. Schneider, J. Ehlers, and E. E. Falco, *Gravitational Lenses*, Springer, Berlin (1992).